# A bio-inspired heterodinuclear hydrogenase CoFe complex

Lili Sun, Suzanne M. Adam, Walaa Mokdad, Rolf David, Anne Milet, Vincent Artero, Carole Duboc

# A bio-inspired heterodinuclear CoFe complex of the hydrogenases

Lili Sun,[a,▪] Suzanne M. Adam,[a,b,▪] Walaa Mokdad,[a] Rolf David,[a] Anne Milet,[a] Vincent Artero,[b,*] Carole Duboc[a,*]

[†] *Univ Grenoble Alpes, CNRS UMR 5250, DCM, F-38000 Grenoble, France*

[‡] *Univ Grenoble Alpes, CNRS, CEA, Laboratoire de Chimie et Biologie des Métaux, F-38000 Grenoble, France*

[▪] *equal contribution of the co-authors*

***Abstract*.** Herein, a new heterobimetallic CoFe complex is reported with the aim of comparing its performance in terms of $H_2$ production within a series of related MFe complexes (M = Ni, Fe). The fully oxidized $[(L^{N2S2})Co^{II}(CO)Fe^{II}Cp]^+$ complex (**$Co^{II}Fe^{II}$**, $L^{N2S2\ 2-}$ = 2,2'-(2,2'-bipyridine-6,6'-diyl)bis(1,1'-diphenylethanethiolate), $Cp^-$ = cyclopentadienyl anion) can be (electro)chemically reduced to its **$Co^{I}Fe^{II}$** form, and both complexes have been isolated and fully characterized by means of classic spectroscopic techniques and theoretical calculations. The redox properties of **$Co^{II}Fe^{II}$** have been investigated in DMF, revealing that this complex is the easiest to reduce by one-election among the analogous MFe complexes (M = Ni, Fe, Co). Nevertheless, it displays no electrocatalytic activity for $H_2$ production, contrary to the FeFe and NiFe analogs, which have proven remarkable performance.

**Introduction**. Hydrogenases are metalloenzymes present in certain organisms, bacteria or microalgae, which have the capacity to produce or oxidize hydrogen.[1-4] Remarkably, they reversibly catalyze the conversion of protons into molecular hydrogen at a potential close to the thermodynamic potential ($E^0_{app}(H^+/H_2)$ = – 413 mV in water at pH 7 and 25 °C under 0.1 bar of $H_2$). Two main classes of hydrogenases are known, differing by the nature of their active sites. The active site of the [NiFe]-hydrogenases consists of a heterodinuclear NiFe complex, where the two metal ions are bridged by thiolate moieties from the cysteine residues of the polypeptide chain. In the case of the [FeFe]-hydrogenases, the active site is a dinuclear iron complex with the two Fe ions also connected by two thiolate functionalities, but arising from an unusual ligand in biology, i.e., dithiomethylamine. These two organometallic MFe clusters (M = Ni or Fe) present a unique structure in biology with the presence of carbon monoxide (CO) and cyanide ($CN^-$) as iron ligands. These structures contribute to these systems' unique electronic properties, which facilitate the protonation of the metal sites under mild conditions, thereby making hydrogenases great catalysts for $H_2$ production. Thus, mimicking the activity of these enzymes with bio-inspired complexes to develop new catalysts for $H_2$ production quickly emerged as an attractive strategy for chemists.[5-8]

Recently, we have described the $H_2$ production reactivity of two dinuclear $M^{II}Fe^{II}$ (M = Fe or Ni) complexes with similar structures. We have demonstrated that both $[(L^{N2S2})Ni^{II}Fe^{II}Cp(CO)]^+$ (**$Ni^{II}Fe^{II}$**)[9, 10] and $[(L^{N2S2})(MeCN)Fe^{II}(CO)Fe^{II}Cp]^+$ (**$Fe^{II}Fe^{II}$**)[11, 12] complexes ($L^{N2S2}$: 2,2'-(2,2'-bipyridine-6,6'-diyl)bis(1,1'-diphenylethanethiolate), Cp = cyclopentadienyl, Scheme 1) display comparable electrocatalytic performance for $H_2$ production, both following an E[ECEC] catalytic mechanism (E = electron transfer, C = chemical reaction, e.g., a protonation step in the present case). This absence of notable changes in the reactivity was rationalized by the non-innocent

redox activity of the $L^{N2S2}$ ligand that is proposed to dominate the catalytic process.[13] Since it has been shown that Co complexes can display high performance for $H_2$ production,[14-17] we describe herein the investigation of the **$Co^{II}Fe^{II}$** parent complex, with the aim of comparing its reactivity with its NiFe and FeFe analogs. The target $[(L^{N2S2})Co^{II}(CO)Fe^{II}Cp]^+$ complex, **$Co^{II}Fe^{II}$**, has been synthesized and characterized, and its reduction chemistry as well as its $H_2$ production reactivity have been investigated.

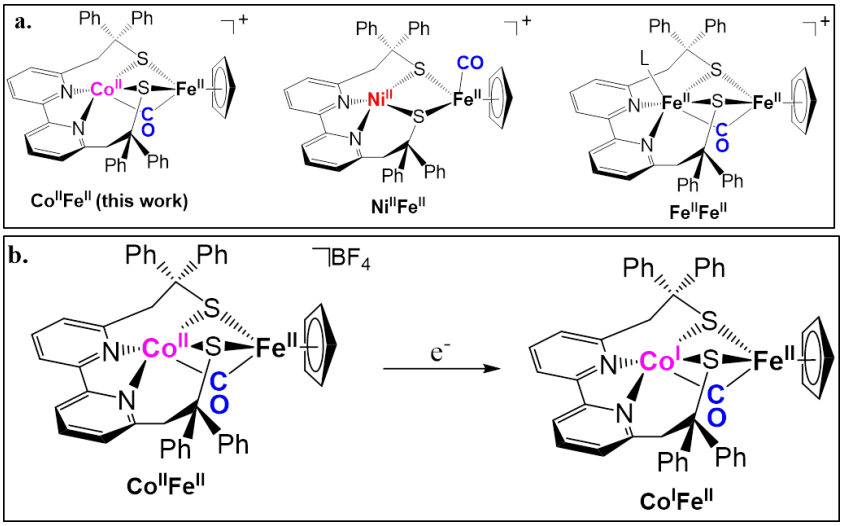


**Scheme 1**. (a) Family of dinuclear model complexes (CoFe (this work), NiFe,[11] and FeFe[10] with L = CO or solvent). (b) Reduction reactivity of the $Co^{II}Fe^{II}$ complex described in this work.

## Results and Discussion

**Synthesis and characterization of $Co^{II}Fe^{II}$.** An equimolar mixture of $[Co^{II}(L^{N2S2})]$ and $[Fe^{II}(CO)(Cp)(CH_3CN)_2]BF_4$ stirred overnight in dichloromethane (DCM) at room temperature under inert atmosphere affords the dark brown $[(L^{N2S2})Co^{II}(CO)Fe^{II}(Cp)]BF_4$ target complex (**$Co^{II}Fe^{II}$**), which could be isolated in high yield (Scheme 2). The optical spectrum of a solution of **$Co^{II}Fe^{II}$** in dimethylformamide (DMF) displays two features in the visible region of the spectrum with $\lambda_{max}$ = 468 nm ($\varepsilon$ = 4900 $M^{-1}cm^{-1}$) and 584 nm ($\varepsilon$ = 3100 $M^{-1}cm^{-1}$), distinct from the spectra of the mononuclear reagents (see Figure S1). The ESI mass spectrum supports the overall formulation, $[(L^{N2S2})Co^{II}Fe^{II}(CO)(Cp)]^+$, with the major mass peak being observed at m/z = 786.04 (calc. 786.09).

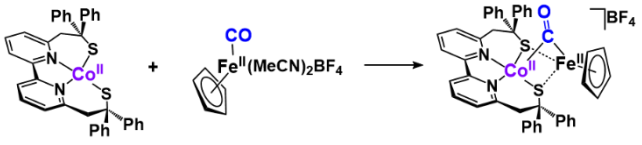


**Scheme 2**. Synthetic pathway to afford **$Co^{II}Fe^{II}$**.

Infrared spectroscopy was employed to monitor the binding mode of the CO moiety in **Co$^{II}$Fe$^{II}$**. A stretching frequency is observed at 1856 cm$^{-1}$ in the range for metal-bridging CO moieties (Figure 1), at an energy close to that found in the **Fe$^{II}$Fe$^{II}$** derivate (1822 cm$^{-1}$), and at a significantly lower energy than the terminal M-CO stretching frequencies present in the [Fe$^{II}$(CH$_3$CN)$_2$(CO)(Cp)]BF$_4$ reagent[18] and the analogous **Ni$^{II}$Fe$^{II}$** complex [9] (1984 and 1929 cm$^{-1}$, respectively). Based on these data, it can be concluded that the CO bridges the Co$^{II}$ and Fe$^{II}$ ions in **Co$^{II}$Fe$^{II}$**, both in solution (see Figure S2) and in the solid state (Figure 3, bottom).

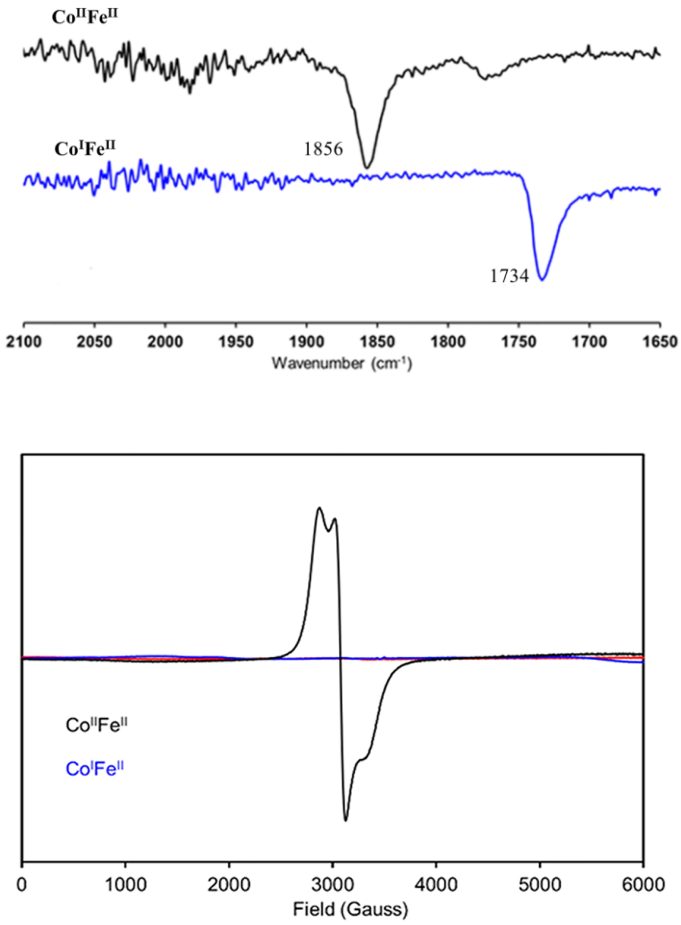


**Figure 1.** Attenuated total reflectance infrared (top) and 100 K solid-state EPR (bottom) spectra of **Co$^{II}$Fe$^{II}$** (black) and **Co$^{I}$Fe$^{II}$** (blue) complexes.

In order to gain insights into the electronic structure of this heterodinuclear complex, EPR spectra were recorded both as a powder sample (Figure 1) and as a frozen DMF solution (Figure S2) sample at 100 K. The solid-state sample clearly shows a rhombic spectrum ($g_x$ = 2.24; $g_y$ = 2.09; $g_z$ = 1.98) consistent with a low-spin $d^7$ Co$^{II}$ species. In this case, the $d^6$ Fe$^{II}$ center does not contribute to the spectrum indicating that the single unpaired electron of the overall $S$ = ½ complex is localized on the Co center. A hyperfine interaction ($I$ = 7/2 for $^{59}$Co) is resolved in the frozen DMF solution sample spectrum, supporting the Co$^{II}$ assignment (see SI, Figure S2).

To further investigate the structural and spectroscopic properties of **Co$^{II}$Fe$^{II}$**, DFT calculations have been carried out. Its optimized structure, **Co$^{II}$Fe$^{II}$***, displays predicted spectroscopic parameters consistent with the experimental ones, especially regarding the calculated $\nu_{CO}$ vibration at 1887 cm$^{-1}$ (*vs* $\nu_{CO}$ exp at 1856 cm$^{-1}$). The overall spin state of the complex is confirmed to be a doublet (the quartet is predicted to be at a much higher energy, see Table S1). The Mulliken spin population of 1.1 on the Co ion is fully consistent with a localized S = ½ Co$^{II}$Fe$^{II}$ complex, as proposed by the experimental EPR data (see Figure S3 for the spin density).

**Redox properties of Co$^{II}$Fe$^{II}$**. The cyclic voltammogram (CV) of a DMF solution of **Co$^{II}$Fe$^{II}$** reveals two diffused-controlled (quasi-)reversible one-electron processes, centered at $E_{1/2}$ = –1.00 V ($\Delta E$p = 100 mV) and $E_{1/2}$ = –2.04 V ($\Delta E$p = 80 mV) vs. Fc$^{+/0}$ (Figure 2). The redox system at –1.00 V can be attributed to the Co$^{II/I}$ reduction, and that at more negative potential, to the reduction of the redox-non-innocent bipyridine ligand. The Co$^{II/I}$ reduction potential against ferrocene, obtained via DFT (see SI for details and Table S2) is in perfect agreement with a value of –1.02 V vs Fc$^{+/0}$.

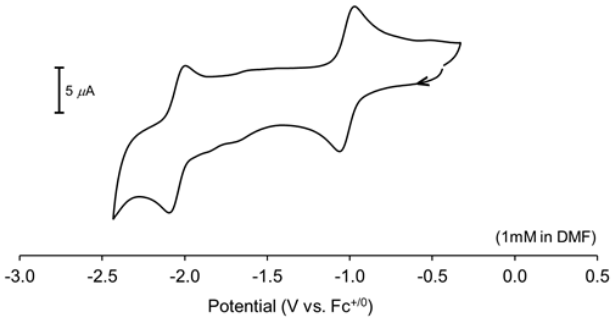


**Figure 2.** Cyclic voltammogram of a DMF solution of **Co$^{II}$Fe$^{II}$** (1 mM); electrolyte: 0.1 M $(Bu)_4NClO_4$; reference: $Ag/AgNO_3$; counter: Pt wire; scan rate: 100 mV s$^{-1}$.

Such assignments can be proposed based on the comparison of its redox properties to those of the analogous **Fe$^{II}$Fe$^{II}$** and **Ni$^{II}$Fe$^{II}$** complexes.[9, 11] The CV of **Ni$^{II}$Fe$^{II}$** reported in MeCN shows two reversible redox systems at –1.29 V and –1.90 V vs. Fc$^{+/0}$, attributed to the Ni$^{II/I}$ and L$^{N2S2}$ reduction processes, respectively. The reduction of the Ni$^{II}$ ion in **Ni$^{II}$Fe$^{II}$** occurs at a significantly more positive potential than in the mononuclear [Ni$^{II}$(L$^{N2S2}$)] complex under the same conditions ($E_{1/2}$ = −1.82 V corresponding to a potential shift of 530 mV), highlighting the strong electronic effect of the Lewis acidic Fe component. The Co$^{II/I}$ reduction potential in **Co$^{II}$Fe$^{II}$** is shifted to an even greater extent (700 mV) as compared to the mononuclear [Co$^{II}$(L$^{N2S2}$)], which displays a quasi-reversible Co$^{II/I}$ wave at –1.7 V in DMF.[14] Regarding **Fe$^{II}$Fe$^{II}$**, the diiron analog exists as the *mono*-CO form in acetonitrile at a concentration of 0.2 mM, with a bridging CO ligand similar to that found in **Co$^{II}$Fe$^{II}$** (see Scheme 1). Under these conditions, the first one-electron reduction process occurs at –1.21 V vs. Fc$^{+/0}$ resulting in the delocalized, mixed-valent Fe$^{1.5}$Fe$^{1.5}$ species. In this series of M$^{II}$Fe$^{II}$ complexes, **Co$^{II}$Fe$^{II}$** is, therefore, the easiest to reduce.

In the analogous **Fe$^{II}$Fe$^{II}$** and **Ni$^{II}$Fe$^{II}$** complexes, it was shown that the second one-electron reduction process occurs at the bipyridine moiety of the L$^{N2S2}$ ligand, at $E_{1/2}$ = –1.65 V and $E_{1/2}$ =

–1.90 V, respectively, in MeCN. In the case of **Co$^{II}$Fe$^{II}$**, the redox system associated with the bipyridine ligand occurs at a less negative potential, $E_{1/2}$ = – 2.04 V in DMF. The small difference with **Ni$^{II}$Fe$^{II}$** can be explained by the difference in the solvent (DMF vs. acetonitrile), while that with **Fe$^{II}$Fe$^{II}$** likely arises from differences in the structural and electronic properties of the one-electron reduced species (see below).

**Synthesis and characterization of the one-electron reduced Co$^{I}$Fe$^{II}$ species.** The **Co$^{II}$Fe$^{II}$** complex can be chemically reduced using one molar equiv. of cobaltocene ($CoCp_2$), to generate the one-electron reduced species **Co$^{I}$Fe$^{II}$** (see SI for details). Based on the electrochemical analysis, it has been proposed that the reduction occurs at the cobalt center. This conclusion is experimentally supported by the disappearance of the X-band EPR feature present in the spectrum of **Co$^{II}$Fe$^{II}$** (Figure 1). The EPR-silent spectrum of **Co$^{I}$Fe$^{II}$** thus confirms an overall $S$ = 0 complex (Co$^{I}$, $d^8$; Fe$^{II}$, $d^6$). The IR spectrum displays a CO vibrational frequency at 1734 cm$^{-1}$ consistent with a bridging mode (Figure 1). With respect to **Co$^{II}$Fe$^{II}$** (1856 cm$^{-1}$) the energy of this vibration is notably weaker, indicating an elongation of the bridging C=O bond. Distinct changes in the optical profile are also observed upon reduction (Figure 3), including the growth of a broad, low-energy d-d transition feature (950 nm; $\varepsilon$ = 1500 M$^{-1}$cm$^{-1}$).

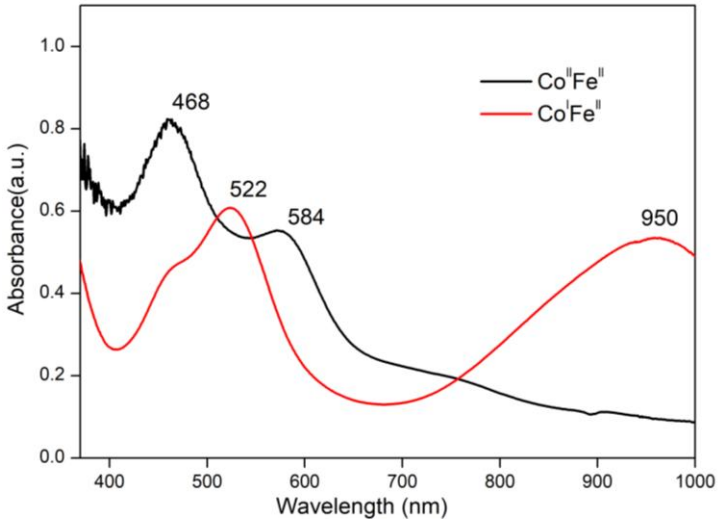


**Figure 3.** UV-visible spectra of the **Co$^{II}$Fe$^{II}$** (black), **Co$^{I}$Fe$^{II}$** (red) complexes (0.1 mM, DMF).

The structural and spectroscopic properties of **Co$^{I}$Fe$^{II}$** have been further investigated by DFT calculations. The predicted CO vibration calculated from its optimized structure, **Co$^{I}$Fe$^{II}$***, is consistent with the experimental ones, i.e., $\nu_{CO}$ vibration at 1779 cm$^{-1}$ *vs* $\nu_{CO}$ exp at 1734 cm$^{-1}$. The overall spin state of the complex is confirmed to be a singlet in agreement with the EPR-silent spectrum.

**Reactivity of Co$^{II}$Fe$^{II}$ in the presence of H$^{+}$.** Following the addition of $Et_3NHBF_4$ as a proton source, a catalytic process ($E_{cat}$ = −1.99 V vs. Fc/Fc$^{+}$, measured at the half-wave) develops on top of the second wave of the **Co$^{II}$Fe$^{II}$** complex (Figure 4). Nevertheless, when compared with the CVs recorded under the same conditions, but in absence of **Co$^{II}$Fe$^{II}$**, the reduction appears to occur at a similar potential evidencing that the presence of **Co$^{II}$Fe$^{II}$** has a marginal impact, if any, on the $H_2$ production catalyzed by the glassy carbon surface of the electrode. This electrochemical behavior was completely unexpected since the investigation of both **Ni$^{II}$Fe$^{II}$** and

**Fe$^{II}$Fe$^{II}$** supported the fact that the nature of the metal bound by the $L^{N2S2}$ ligand has no notable impact on the performance of these electrocatalysts and that the bipyridine unit was the key factor in controlling their reactivity.[11]

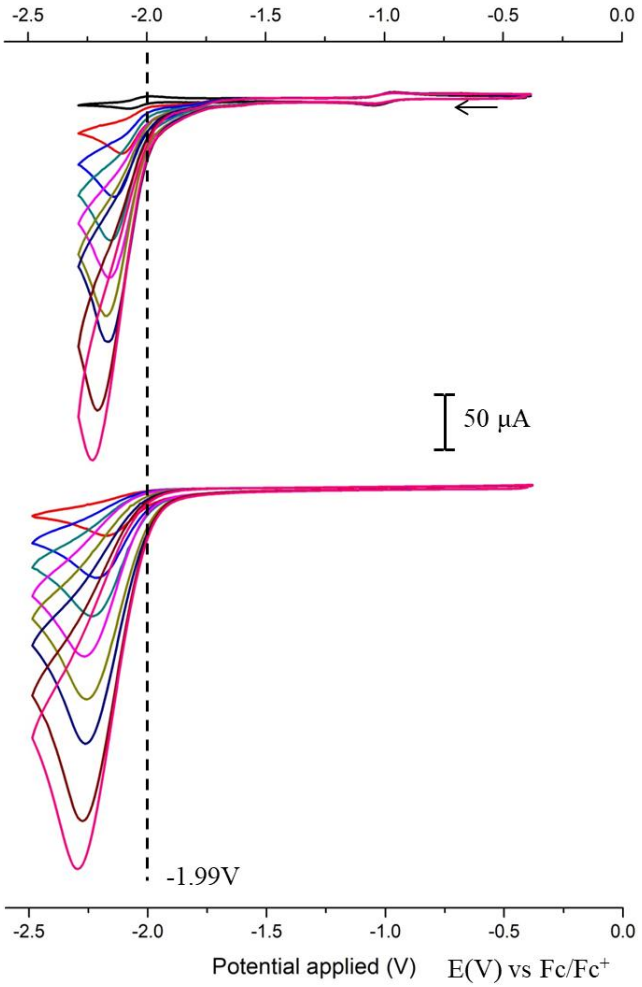


**Figure 3.** CVs of **Co$^{II}$Fe$^{II}$** (0.73 mM, top, black) in the absence or presence of various amounts of $Et_3NHBF_4$ in DMF solution, 0.1 M n-$Bu_4NClO_4$, on a glassy carbon electrode at 100 mv $s^{-1}$. 5 equiv. (red); 10 equiv. (blue); 15 equiv. (cyan); 20 equiv. (pink); 25 equiv. (dark yellow); 30 equiv. (dark blue); 40 equiv. (deep red); 50 equiv. (magenta). The CVs of the corresponding blank samples (no catalyst) are also shown (bottom).

**Conclusions.** The target **Co$^{II}$Fe$^{II}$** complex was synthesized with the aim of comparing its reactivity towards $H_2$ production with its NiFe and FeFe analogs. We were also able to isolate and characterize the corresponding one-electron reduced species. Unexpectedly, this new complex was not active to produce $H_2$ electrocatalytically, while the analogous NiFe and FeFe complexes have demonstrated remarkable performance. Current work in our laboratories focuses on understanding the origin of this lack of reactivity, since **Co$^{II}$Fe$^{II}$** displays the most promising redox properties, i.e., it is the easiest to reduce within the series of M$^{II}$Fe$^{II}$ complexes.

**Acknowledgments**. Financial support for this work was provided by the Agence National de la Recherche in the framework of the “Investissements d’avenir” Program (ANR- 15-IDEX-02), the Labex ARCANE (ANR-11-LABX-003), and the CBH-EUR-GS(ANR-17-EURE-0003), and ANR-DFG (ANR-16-CE92_0012_01 NiFeMim) and the China Scholarship Council.

**References:**

1. W. Lubitz, H. Ogata, O. Rüdiger and E. Reijerse, *Chem. Rev.*, 2014, **114**, 4081-4148.
2. D. Schilter, J. M. Camara, M. T. Huynh, S. Hammes-Schiffer and T. B. Rauchfuss, *Chem. Rev.*, 2016, **116**, 8693-8749.
3. Y. Nicolet, C. Piras, P. Legrand, C. E. Hatchikian and J. C. Fontecilla-Camps, *Structure*, 1999, **7**, 13-23.
4. A. Volbeda, M.-H. Charon, C. Piras, E. C. Hatchikian, M. Frey and J. C. Fontecilla-Camps, *Nature*, 1995, **373**, 580-587.
5. S. Kaur-Ghumaan and M. Stein, *Dalton Trans.*, 2014, **43**, 9392-9405.
6. A. C. Ghosh, C. Duboc and M. Gennari, *Coordination Chemistry Reviews*, 2021, **428**, 213606.
7. N. Coutard, N. Kaeffer and V. Artero, *Chem. Commun.*, 2016, **52**, 13728-13748.
8. J. T. Kleinhaus, F. Wittkamp, S. Yadav, D. Siegmund and U.-P. Apfel, *Chemical Society Reviews*, 2021, **50**, 1668-1784.
9. D. Brazzolotto, M. Gennari, N. Queyriaux, T. R. Simmons, J. Pécaut, S. Demeshko, F. Meyer, M. Orio, V. Artero and C. Duboc, *Nat. Chem.*, 2016, **8**, 1054–1060.
10. M. E. Ahmed, S. Chattopadhyay, L. K. Wang, D. Brazzolotto, D. Pramanik, D. Aldakov, J. Fize, A. Morozan, M. Gennari, C. Duboc, A. Dey and V. Artero, *Angew. Chem. Int. Ed.*, 2018, **57**, 16001-16004.
11. L. Wang, M. Gennari, A. Barrozo, J. Fize, C. Philouze, S. Demeshko, F. Meyer, M. Orio, V. Artero and C. Duboc, *ACS Catal.*, 2020, **10**, 177-186.
12. M. E. Ahmed, D. Saha, L. Wang, M. Gennari, S. Ghosh Dey, V. Artero, A. Dey and C. Duboc, *ChemElectroChem*, 2021, **8**, 1674-1677.
13. M. Gennari and C. Duboc, *Acc. Chem. Res.*, 2020, **53**, 2753-2761.
14. V. Artero and J.-M. Saveant, *Energy & Environmental Science*, 2014, **7**, 3808-3814.
15. G.-G. Luo, H.-L. Zhang, Y.-W. Tao, Q.-Y. Wu, D. Tian and Q. Zhang, *Inorganic Chemistry Frontiers*, 2019, **6**, 343-354.
16. N. Queyriaux, R. T. Jane, J. Massin, V. Artero and M. Chavarot-Kerlidou, *Coordination Chemistry Reviews*, 2015, **304-305**, 3-19.
17. D. Dolui, S. Khandelwal, P. Majumder and A. Dutta, *Chem. Commun.*, 2020, **56**, 8166-8181.
18. A. R. Cutler and A. B. Todaro, *Organometallics*, 1988, **7**, 1782-1787.